Revised Manuscript (clean for typesetting) Click here to view linked References

SELECTIVE C2 ELECTROCHEMICAL SYNTHESIS FROM METHANE ON MODIFIED ALUMINA SUPPORTING SINGLE ATOM CATALYSTS

Eleonora Ponticorvo[1,2*], Mariagrazia Iuliano[3], Claudia Cirillo[1,2], Maria Sarno[1,2]

[1]Department of Physics "E.R. Caianiello" University of Salerno, Via Giovanni Paolo II ,132 - 84084 Fisciano (SA), Italy.
[2]NanoMates, Research Centre for Nanomaterials and Nanotechnology at the University of Salerno, University of Salerno, Via Giovanni Paolo II ,132 - 84084 Fisciano (SA), Italy.
[3]Department of Industrial Engineering, University of Salerno, via Giovanni Paolo II, 132 - 84084 Fisciano (SA), Italy

ABSTRACT

The production of C2 compounds in an aqueous solution by efficient and selective electro-conversion of methane is a challenge and of great significance topic. Here, enhanced catalysts, with tunable electrocatalytic activities with time, for direct and selective oxidation of methane to C2 products (i.e., acetic acid and ethanol) at ambient temperature were prepared by exploiting Rh and Cu single atoms dispersed on NH_4BF_4 modified Al_2O_3 nanoparticles exhibiting a large amount of Brønsted acid sites. Brønsted acid sites play a pivotal role in the final formation allowing the direct CO insertion into reaction intermediates. A high acetic acid production, over the Rh-based electrocatalyst, of 33.57 μmol/hcm^2 after only 40 min of reaction was obtained. On the other hand, a selective ethanol production rate of 37.14 μmol/hcm^2 after 120 min of reaction was achieved over the Cu-based catalyst, thanks to the tendency vs. acetyl species formation over copper single atoms. Catalysts activity was kept stable for at least 120 min, at 2 V, and ambient temperature. The comparative analysis with the literature results highlights the high efficiency of our catalysts in selectively promoting acetic acid and ethanol productions with high yields, and stability. A novel way, exploiting single-atoms dispersed on suitable supports, for the production of performing surfaces, was provided.

Keywords: methane conversion, Rh single atom, Cu single atom, Al_2O_3 nanoparticles, acetic acid, ethanol, electrochemical conversion.

*Corresponding author: Tel.: +39 089 963460; E-mail address: eponticorvo@unisa.it (E.Ponticorvo).

1. Introduction

Methane (CH_4) is the main hydrocarbon component of natural gas, biogas, shale gas, and clathrates [1-3]. According to the BP Statistical Review of World Energy, global natural gas production of 3,854 billion m^3 in 2020 was reached [4]. Methane is the major feedstock for the industrial production of syngas or hydrogen through the steam methane reforming (SMR) process. SMR involves high temperature and pressure, is energy-intensive, and with large amounts of associated carbon emissions. Furthermore, to gain economic benefits, these processes need to operate at a large scale, typical plants size of ~ 2000 to 3000 metric tons per day (MTD). However, some methane resources, such as shale gas and clathrates, are found in small amounts and/or located in remote areas, which require uneconomic energy inputs to liquefy for transportation over long distances [5]. Therefore, new technologies for small-scale and highly distributed production of high-value chemicals from methane oxidation are in high demand. Methane is inherently difficult to activate [6] because of chemical inertness and lack of polarity. Although, it has been the object of a lot of studies, the direct conversion of methane, through homogeneous and heterogeneous catalysis, is still a challenge.

Electrocatalytic approaches represent promising alternatives [7], overcoming the methane chemical inertness thanks to the fast formation of highly reactive compounds [8,9], and supplying partially oxidized stable products at relatively low temperatures. Therefore, a convenient procedure to convert CH_4 into liquid chemicals using electricity generated from renewable sources, like solar or wind, would be an excellent approach. In this case, a suitable catalyst for product selection and activity maintenance, i.e., avoiding the deposition of poisoning carbonaceous materials, must be designed. In particular, an efficient catalyst should provide several functions: methane adsorption and activation; oxygen activation; selectivity for the desired compounds, and stability against further oxidation. To date, mainly C1 compounds as dominant products were obtained by CH_4

electro-oxidation processes. Efficient electrochemical production of C2 products, i.e. acetic acid and ethanol, is also of great importance [10-16]. Therefore, advanced electrocatalysts, enabling selectively C-H activation and C-C coupling, are highly desirable for CH_4 electro-oxidation. Supported single atom metals, maximizing atom efficiency, have been demonstrated as promising materials for C-H bond activation [17,18]. On the other hand, the exploitation of single atoms [19-24], without bulky surface influencing negatively catalysis and causing additional diffusive limitations, is a fascinating route.

Rhodium-based catalysts exhibited outstanding catalytic activities in heterogeneous methane oxidation reactions [18,25,26]. In particular, Rh nanoclusters with unsaturated coordinate atoms can stabilize $\cdot CH_3$ species, thus avoiding its further oxidation to CO_2 [27]. On the other hand, a literature survey shows that Cu is a key component in obtaining multicarbon products [28-38]. Besides the low price, the most prominent advantage of copper-based catalysts was their inherent inertness of C-C bond hydrogenolysis, restraining the complete oxidation of methane [39]. To convert methane into C2 compounds, a tandem oxidation/carbonylation reaction sequence must occur. Carbonylation, to form metal–$COCH_3$ species, requires acidic surfaces. In particular, Brønsted acid sites play a pivotal role in allowing direct CO insertion into metal–CH_3 bonds.

Aluminum oxides (Al_2O_3) are a class of advantaged materials with widespread applications as adsorbents and catalysts [40,41]. Particularly, γ-Al_2O_3 is one of the most employed supports for heterogeneous industrial catalysis. The assets of alumina include low cost, relatively high surface area, large porosity, and good chemical and thermal stability [42]. Al_2O_3 also possesses special surface properties that certainly affect the ability of the catalytic systems [43]. Moreover, a simple NH_4BF_4 modification allows obtaining an improved amount of Brønsted acid sites.

Herein, to develop enhanced catalysts for direct and selective oxidation of methane at room temperature, Rh and Cu single atoms dispersed on, alumina modified by Brønsted acid sites, were prepared. We have found that the nanocatalysts can catalyse efficiently the selective oxidation of CH_4 to acetic acid and ethanol.

2. Experimental

2.1 Synthesis of M/Al_2O_3 catalyst

All chemicals were acquired from Sigma Aldrich and used as received without further treatment. The synthesis of γ-Al_2O_3 supported M (M/Al_2O_3, where M=Rh, and Cu; 1 wt. % of M) was carried out by an impregnation method [44]. Briefly, 300 mg of γ-Al_2O_3 was added to two aqueous solutions (20 ml) containing rhodium nitrate ($Rh(NO_3)_3$, Sigma Aldrich), or copper nitrate ($Cu(NO_3)_2$, Sigma Aldrich). The solutions were stirred for 120 min, and, after, the water was removed by a vacuum rotary evaporator (Hei-VAP Core, Heidolph). Finally, the obtained materials were dried at 105°C overnight and then calcined at 500°C for 180 min in air.

2.2 Modification of M/Al_2O_3 catalyst with Brønsted acid sites

Rh/Al_2O_3, and Cu/Al_2O_3 catalysts modified with Brønsted acid sites were prepared by a sol−gel route. In particular, 150 mg of M/Al_2O_3 were dispersed in 40 mL of distilled water (DW) and vigorously stirred, and 35 ml of NH_4BF_4 aqueous solution (1.85 mg/ml) was added to the suspension at 85°C. Nitric acid (1 M) was dropwise added to the suspension until pH=3 (the pH solution was measured with a 3510 pH meter (Jenway)). The suspension was vigorously mixed for 2 h at 85°C. After, to reach pH 6, aqueous ammonia was dropwise added into the solution under stirring. The suspension was dried at 75°C for 24 h in air. The gel obtained was then washed with DW and dried at 85°C for 48 h. Finally, the sample was calcinated at 550°C for 4 h to obtain $Rh/Al_2O_3@NH_4BF_4$, and $Cu/Al_2O_3@NH_4BF_4$ catalysts.

2.3 Electrochemical of CH_4 oxidation reaction

The electrochemical oxidation of CH_4 was conducted in a two-electrode assembly. A graphite foil (area =10 cm^2) and a Pt foil (area =10 cm^2) were used as the working electrode, and the counter electrode, respectively. 30 ml of 0.5 M $KHCO_3$ solution was used as an electrolyte. The reactor was a closed cell. The working electrode was prepared by dispersing the catalyst in DW with a concentration of 4 mg/ml and then dropping the solution on the surface of the graphite foil. After drying, a 5% Nafion 117 solution was dropped to cover the sample, followed by drying at room temperature. Before the electrochemical reaction, the electrolyte was bubbled with CH_4 for 30 min to remove the oxygen and fill the space in the reaction instrument. After that, the instrument was quickly closed to prevent gas emissions. The reaction temperature was controlled by a water bath, which was maintained at 25°C.

2.4 Characterization

The Rh/Al_2O_3, and Cu/Al_2O_3 catalysts were analyzed by SEM (TESCAN-VEGA LMH; 230 V) analysis. Transmission electron microscopy (TEM) images were obtained by an FEI Tecnai electron microscope (200 kV). High-resolution analytical TEM (F20 FEI Tecnai-200 kV) was used for high-angle annular dark-field (HAADF) analysis. HAADF detector was employed in STEM mode. XPS measurements were obtained with a PHI-550 Multitechnique spectrometer. X-ray diffraction measurements were performed by a Bruker D2 Phaser X-ray diffractometer, using CuK_α radiation. TGA 2, METTLER TOLEDO was used for thermogravimetric analysis (TG-TDG). For Diffuse Reflectance Infrared Fourier Transform Spectroscopy (DRIFTS) measurements, a spectrometer from Thermo Scientific Nicolet (i550 FTIR) was used. For the measurements, a flow of CO (20 mL/min) was fed to the reaction chamber, followed by a purge flow of nitrogen to remove CO in the gas phase. After modification with NH_4BF_4, Rh/Al_2O_3, and Cu/Al_2O_3 catalysts were analyzed by FT-IR spectra a Nicolet iS50 was used. The spectra of the samples were recorded by

accumulating 32 scans at 4 cm^{-1} resolutions. The surface acidities of modified Rh/Al_2O_3, and Cu/Al_2O_3 catalysts were determined by FT-IR analyses after pyridine adsorption [45]. For NH_3-TPD (NH_3-Temperature-Programmed Desorption) an all-glass experimental apparatus coupled with a TCD (thermal conductive detector) was used. The methane oxidation products were recorded by ^{1}H-NMR measurements, performed with a Bruker Advance 300 (Operating at 300 MHz). In particular, the samples were prepared by mixing 0.4 ml of the solutions with 0.2 ml of D_2O. The amount of CH_4 and other gaseous products (CO, CO_2, etc..) were determined by GC–MS instrument (Thermo-Fischer).

A titration method, to quantify Rh and Cu single atoms, was used [46,47]. In particular, leaching of the eventually larger aggregates was promoted. For the leaching, the temperature was adjusted to avoid support dissolution. In particular, the leaching procedure was developed at room temperature [48], to selectively dissolve Rh and Cu clusters without removing isolated Rh and Cu atoms. The leaching process was executed by suspending 100 mg of the catalyst in 10 mL of 2 M HCl/1% H_2O_2 solution under stirring for 8 h at 25 °C. The sample was then washed in distilled water, separated by centrifugation, and dried at 90 °C for 5 h.

3. Results and Discussion

3.1 Characterization of the electrocatalysts

Figures 1 and 2 show TEM analysis of Rh/Al_2O_3 and Cu/Al_2O_3. For both samples, the images show particles with a diameter of a few nanometers. The average particle sizes were carefully evaluated by analyzing 100 particles randomly taken from TEM images for each catalyst. An average particle size of 3.1 ± 0.6 nm was obtained for alumina nanoparticles in both samples. The aberration-corrected HAADF/STEM image of Rh/Al_2O_3 is shown in Figure 1. Contrast points, coherent with single rhodium atoms, can be seen. The elements mapping images, shown in EDX analyses (Figure 1), indicated the homogeneous distribution of Rh elements in the sample. Moreover, EDX provided also the

Al and O maps, which are practically superimposable, supplying evidence of the homogenous distribution of the elements [49,50]. The aberration-corrected HAADF/STEM image of Cu/Al_2O_3 is shown in Figure 2, highlighting contrast points, coherent with single copper atoms. TEM-EDX maps of Cu/Al_2O_3 also shown in Figure 2 indicate the homogeneous distribution of Al, O, and Cu. Al/Rh and Al/Cu atomic ratios, according to EDX evaluation, are equal to, 39.94/0.15 and 39.91/0.2, respectively, in good agreement with the amount of precursors used for synthesis.

Rh and Cu were examined by CO-DRIFTS at room temperature (Figure 3). CO symmetrical and asymmetrical stretching due to $Rh(CO)_2$ species (Figure 3a), with mononuclear Rh on Al_2O_3, can be seen at 2107 cm^{-1} and 2040 cm^{-1} (Figure 3a). Broad atop and bridged peaks are barely perceptible at 2068 cm^{-1} and 1867 cm^{-1} probably due to the presence of Rh clusters [51]. Cu/Al_2O_3 was examined in the wavelength range of 2000-2300 cm^{-1} [52]. A weaker band at 2171 was assigned to CO linearly adsorbed on Cu^{2+} [53] (Figure 3b), and barely visible bands at 2116 and 2054 cm^{-1} (Figure 3b) were attributed to the linear adsorption of CO on Cu^{+} and Cu^{0}, respectively. On the other hand, Cu^{2+}-CO species were generally weakly bound, which can be observed only below ambient temperature [54]. Isolated rhodium and copper were estimated to be 96 and 98 %, respectively, by applying a titration approach [46].

The XRD patterns of Rh/Al_2O_3, and Cu/Al_2O_3 samples were shown in Figure 4. The X-ray diffraction patterns were acquired in the 2θ range of 20-80º. The two profiles differ little due to a sample holder halo and the powder amounts used for the measurements. The results indicate some crystalline phases mixed with the primary amorphous structures of γ-alumina [55].

No Rh, and Cu peaks were detected from the XRD patterns of Rh/Al_2O_3, and Cu/Al_2O_3 (Figure 4), in agreement with the single-atom nature of that Rh and Cu species [56].

The TG-DTG analyses of the different samples were carried out, and the results are displayed in Figure 5. The curves, with soft slopes and without sharp peaks, showed single phases and no impurity in both samples. In particular, slight, but consecutive, weight losses up to 600°C, were observed, which can be ascribed to samples' dehydration and the chemically adsorbed residual hydroxyl species decomposition [57]. In Figure S1 the thermogravimetric profiles of NH_4BF_4 alone, Rh/Al_2O_3, and Cu/Al_2O_3 after modification with NH_4BF_4 are shown for comparison. In particular, the TG curves of $Rh/Al_2O_3@NH_4BF_4$, and $Cu/Al_2O_3@NH_4BF_4$ display a weight loss in the temperature the range between 320 °C and 415 °C due to NH_4BF_4.

XPS analyses (Figure 6) were adopted to detect catalysts' surface composition. The Rh binding energy at $3d_{5/2}$ in Rh/Al_2O_3 catalyst (Figure 6a) was located at 309.6 eV, indicating the Rh^{3+} state of rhodium single atoms [58,59]. In Figure 6b only one peak, at the binding energy of ~934.0 eV, corresponding to Cu^{2+} species [60,61], can be deconvoluted from the corresponding Cu $2p_{3/2}$ XPS signals, suggesting no mixed oxidation states of Cu species in the Cu/Al_2O_3 catalyst.

FT-IR spectroscopy was used to analyze the chemical property of Rh/Al_2O_3, Cu/Al_2O_3, $Rh/Al_2O_3@NH_4BF_4$, and $Cu/Al_2O_3@NH_4BF_4$ (Figure 7). The FT-IR profiles of Rh/Al_2O_3 and Cu/Al_2O_3 samples (Figure 7a) showed slight bands at 3340 cm^{-1} and 3371 cm^{-1}, respectively, assigned to the stretching vibration of hydroxyl groups [62]. The bands at 1636 cm^{-1} and 1630 cm^{-1}, in the Rh/Al_2O_3 and, Cu/Al_2O_3 profiles respectively, can be ascribed to the typical deformation vibration of physically adsorbed water [63]. Finally, the two profiles showed broad bands at about 500 cm^{-1}, attributed to the Al–O bond of alumina [63]. In Figure 7b, the FT-IR profiles of $Rh/Al_2O_3@NH_4BF_4$ and $Cu/Al_2O_3@NH_4BF_4$ are shown. The profiles evidenced the presence of new main bands at ~ 1485 cm^{-1} and 720 cm^{-1}, probably due to the formation of aluminum borate [62]. These results confirmed the modification of Rh/Al_2O_3 and Cu/Al_2O_3 with NH_4BF_4. Acidities for

Al_2O_3, $Rh/Al_2O_3@NH_4BF_4$, and $Cu/Al_2O_3@NH_4BF_4$ samples were monitored by FT-IR pyridine adsorption (Figure 8). Firstly, physically adsorbed pyridine was outgassed at 300°C in nitrogen flow for 3 h. The bands (Figure 8a) at 1445, 1579, 1597, and 1617 cm^{-1} in the spectra of Al_2O_3, $Rh/Al_2O_3@NH_4BF_4$, and $Cu/Al_2O_3@NH_4BF_4$, were ascribed to pyridine species absorbed on Lewis acidic sites [64,65]. The band at 1492 cm^{-1} was assigned to the combined Brønsted and Lewis acid sites. Furthermore, the spectra of Rh/Al_2O_3, and Cu/Al_2O_3 showed new bands at 1546 cm^{-1} and 1642 cm^{-1}, respectively, due to the pyridine absorbed on Brønsted acidic sites, confirming the presence of Brønsted acidic sites [66]. The stability of both acid sites was confirmed by the analysis performed after thermal treatment at 300°C for 1 h, shown in Figure 8b. The strengths of the catalyst acid sites were also monitored through NH_3-TPD (Figure S2) confirming the results obtained by the FT-IR pyridine adsorption. The surface composition of Al_2O_3 is responsible for the surface acidity of the catalyst, the surface of Al_2O_3 was covered with hydroxyl groups bound to sites of various geometries. As reported by Knözinger et al. [67], the surface composition/structure of alumina can be described by five types of surface sites. In Figure 9, the mechanism explaining the formation of a Brönsted acid site on the alumina surface was shown. An -OH group, which can be bounded to two tetrahedral or octahedral aluminum atoms is also depicted. Fluorine modification replaces oxygen groups located on alumina atoms with strong electronegative F atoms. In the meantime, electrons from neighboring atoms were withdrawn leading to a decreased electron cloud density of -OH groups and allowing a much easier proton release, which improves Brönsted sites' acidity. Boron atoms form B−O−Al junctions with under-coordinated aluminum.

3.2 Electrochemical CH_4 conversion

To measure the products from CH_4 oxidation, a two-electrode system was employed with catalyst-loaded carbon paper as the anode, Pt foil as the cathode, and a carbonate solution

as the electrolyte. A sealed reactor instrument, suitable for the conversion and for tracking the CH_4 oxidation progress in real-time, was employed.

Figure 10 shows the linear sweep voltammetry (LSV) curves of the Rh/Al_2O_3 and, Cu/Al_2O_3 catalysts modified with NH_4BF_4. The catalysts showed high electrochemical current densities for CH_4 oxidation. In particular, the current density of the $Cu/Al_2O_3@NH_4BF_4$ catalyst was relatively lower than $Rh/Al_2O_3@NH_4BF_4$. This indicates a higher catalytic activity in CH_4 oxidation, not only at the onset position but along the whole measure, for $Rh/Al_2O_3@NH_4BF_4$ catalyst.

Based on the LSV curves, 2.0 V was selected as the suitable potential for CH_4 electrochemical oxidation to obtain a relatively high current density and low competition with water oxidation. The products were collected separately after reaction at different times. ^{1}H-NMR (proton nuclear magnetic resonance) spectra were obtained to identify the products. GC-MS was employed to analyze CH_4 consumed and the gas phase during the reaction. Moreover, the reference line of the CH_4 amount was also measured by GC-MS. The CH_4 conversion is shown in Figure 11 and Figure 12 for $Rh/Al_2O_3@NH_4BF_4$, and $Cu/Al_2O_3@NH_4BF_4$ catalysts, respectively. The conversion of methane on $Rh/Al_2O_3@NH_4BF_4$ increased quickly at increased reaction times, after 120 min of reaction about 70% of the CH_4 gas in the sealed reactor was oxidized. For $Cu/Al_2O_3@NH_4BF_4$ catalyst the methane conversion efficiency was not appreciable after only 10 min, after that slowly increased, up to ~ 50 %, under time increases. Figure 13 shows the product selectivity at increasing times and 25°C (CO was the only other product, current efficiency of ~ 3%), obtained under $Rh/Al_2O_3@NH_4BF_4$ anode polarization. After 10 min of CH_4 oxidation, the two carbon atoms molecule of acetic acid (AA) was observed, with a small amount of methanol. AA was the main product during the first 60 minutes of reaction, see also the ^{1}H-NMR spectra (Figure 14). A very high rate of acetic acid formation is allowed by our $Rh/Al_2O_3@NH_4BF_4$ electrocatalyst, corresponding to an

acetic acid production of 33.57 μmol/hcm^2 after 40 min of reaction time, with current efficiency of 95%. Moreover, after 90 min of reaction, the amount of acetic acid decreased (Figure 13), and ethanol was produced as the main stable product of methane oxidation. An ethanol production rate of 27.97 μmol/hcm^2 (current efficiency of 51 %) was achieved after 120 min of reaction.

The product selectivity, at increasing times and 25°C (CO was the only other product, the current efficiency of ~ 4%) produced by polarization at the Cu/Al_2O_3@NH_4BF_4 anode, was shown in Figure 15. In this case, acetic acid/ethanol mixture formation was observed after 20 min of CH_4 oxidation, as illustrated by ^{1}H-NMR spectra (Figure 16). The amount of acetic acid decreased with the reaction time (Figure 15), and, ethanol was the main stable product of methane oxidation after 40 min. However, a production rate for the acetic acid of 20.63 μmol/hcm^2, was achieved, with current efficiency of 38%. At 120 min only a small amount of acetic acid was present and 85% of ethanol selectivity was reached, showing an ethanol production rate of 37.14 μmol/hcm^2, achieving 90% current efficiency. Current density-time curves of Rh/Al_2O_3@NH_4BF_4 and Cu/Al_2O_3@NH_4BF_4 catalysts during long-term electrochemical CH_4 oxidation are shown in Figure 17. The curves indicated the stable electrocatalytic CH_4 oxidation process, without the deposition of poisoning carbonaceous materials.

In conclusion, the prepared catalysts, with tuneable electrocatalytic activities with time, showed very promising performance for direct and selective oxidation of methane at low temperatures, producing ethanol or acetic acid, with high selectivity (>90%) [68]. In particular, the analysis of the literature [58, 69-77] results, see Table 1, highlights the high efficiency of our catalyst in selectively promoting target molecules production with high yields.

Al_2O_3 alone and single metal catalysts supported on Al_2O_3 were also tested before the modification with NH_4BF_4, see Figure 18. Al_2O_3 alone exhibits a weaker catalytic activity

(Figure 18a). The behavior of the single metals supported on Al_2O_3 catalysts is in line with the higher tendency of Cu and Rh single atoms to oxidize CH_4 giving methanol (Figure 18b) and confirms that the carbonylation activity increases in the presence of Brønsted acid sites [78,79]. Although the reaction pathway is not completely clear, the most probable path involves a first step in which the M^+ cations facilitate the activation of methane in water to form M–CH_3 species, which can be further functionalized under our reaction conditions. In particular, "CO" species mainly derived from methanol intermediate, thanks to their cleavage in the methanol molecules at the Brønsted acid sites of the framework [80-82], may insert directly into CH_3–M bonds [83], and carbonylate to produce the complex CH_3CO–M, promoted itself by Brønsted acid sites [17]. Finally, the reaction of the acetyl groups with H_2O likely leads to the formation of CH_3COOH [84]. The subsequent ethanol formation can be due to the hydrogenation of the acetic acid. In particular, acetyl species were formed by acetic acid through the breaking of the C-OH bond [39,85], promoting the catalytic conversion of acetic acid to ethanol, through acetyl species hydrogenation. FTIR spectra of Cu/Al_2O_3 and Rh/Al_2O_3 modified with NH_4BF_4 after 90 min of CH_4 electrochemical conversion are provided in Figure S3. Both catalysts show bands at around 1391 cm^{-1} (R−COO−) and 1699 cm^{-1} (R=O) which are attributed to symmetric COO stretching vibrations from absorbed acetic intermediate species, such as acetaldehyde (R−COO−), and acetates/acetic acid (R=O) on the surface of the nanocatalysts [86]. At 1300 cm^{-1} the acetic acid characteristic band is visible [87]. The band at 1425 cm^{-1} represents R−OH species and is assigned to adsorbed ethanol molecules [88]. Strong H-bonding was formed between carbonyl groups and hydroxyl groups of acetic acid, however, $Cu/Al_2O_3@NH_4BF_4$ catalyst, promoting the dissociation of acetic acid into acetyl species thanks to Cu [39] highly dispersed single atoms, favours the catalytic hydrogenation performance significantly. As for $Rh/Al_2O_3@NH_4BF_4$ catalyst, this

phenomenon isn't prevailing [85], leading to a more selective acetic acid formation at shorter times.

4. Conclusion

Enhanced catalysts, with tuneable electrocatalytic activities with time, for fast, direct, and selective oxidation of methane at low temperature, based on Rh and Cu single atoms dispersed on Al_2O_3, were prepared. XPS analysis was performed to detect the surface composition of Rh/Al_2O_3 and Cu/Al_2O_3, the profiles evidence the presence of Al_2O_3. Single atoms of Rh and Cu were also detected. TEM analysis revealed the morphology of the nanomaterials, which are constituted of small nanoparticles of Al_2O_3. Literature analysis evidences the high efficiency of our catalysts in selectively promoting acetic acid and ethanol with high yields. The excellent behavior of our nanocatalysts can be attributed to a combination of aspects. The small Al_2O_3 size allows for electrode wettability, Rh and Cu single atoms inclusions for methane activation, and the key role of the Brønsted acid sites for "CO" species cleavage and carbonylation. $Rh/Al_2O_3@NH_4BF_4$ exhibited up to 70% of CH_4 conversion after only 120 min of reaction time. Very selective acetic acid production was obtained, corresponding to an acetic acid production of 33.57 $\mu mol/hcm^2$ after 40 min of reaction time. In the case of $Cu/Al_2O_3@NH_4BF_4$ anode, favoring acetyl species formation through C-OH bond breaking, a selective ethanol production rate of 37.14 $\mu mol/hcm^2$ was achieved. On the other hand, the behavior of the single metals supported on Al_2O_3 catalysts before the modification with NH_4BF_4 was in line with the higher tendency of Cu and Rh single atoms to oxidize CH_4 giving methanol.

References

1. Q. Miao, G.X. Xiong, S.S. Sheng, W. Cui, L. Xu, X.X. Guo, Partial oxidation of methane to syngas over nickel-based catalysts modified by alkali metal oxide and rare earth metal oxide, Appl. Catal. A Gen. 154 (1997) 17–27. https://doi.org/10.1016/s0926-860x(96)00377-8.
2. M.C. Alvarez-Galvan, N. Mota, M. Ojeda, S. Rojas, R.M. Navarro, J.L.G. Fierro, Direct methane conversion routes to chemicals and fuels, Catal. Today 171 (2011) 15–23. https://doi.org/10.1016/j.cattod.2011.02.028.
3. V.C.-C. Wang, S. Maji, P.P.-Y. Chen, H.K. Lee, S.S.-F. Yu, S.I. Chan, Alkane oxidation: methane monooxygenases, related enzymes, and their biomimetics, Chem. Rev. 117 (2017) 8574-8621. https://doi.org/10.1021/acs.chemrev.6b00624.
4. Statistical Review of World Energy, BP Statistical Review of World Energy https://www.bp.com/en/global/corporate/energy-economics/statistical-review-of-world-energy.html, 2021.
5. M. Ravi, M. Ranocchiari, J.A. van Bokhoven, The Direct Catalytic Oxidation of Methane to Methanol—A Critical Assessment, Angew. Chem. Int. Ed. 56 (2017) 16464–16483. https://doi.org/10.1002/anie.201702550.
6. E.M. Alayon, M. Nachtegaal, M. Ranocchiari, J.A.V. Bokhoven. Catalytic conversion of methane to methanol over Cu–mordenite, Chem. Commun. (Camb.), 48 (2012), pp. 404-406. https://doi.org/10.1039/c1cc15840f.
7. K. Dong, J. Liang, Y.Y. Wang, Y.C. Ren, Z.Q. Xu, H.P. Zhou, L. Li, Q. Liu, Y.L. Luo, T.S. Li, A.M. Asiri, Q. Li, D.W. Ma, X.P. Sun, Plasma-induced defective TiO_2-x with oxygen vacancies: A high-active and robust bifunctional catalyst toward H_2O_2 electrosynthesis, Chem Catalysis 1 (2021), pp. 1437-1448. https://doi.org/10.1016/j.checat.2021.10.011.
8. K.J. Lee, J.L. Dempsey. When Electrochemistry Met Methane: Rapid Catalyst Oxidation Fuels Hydrocarbon Functionalization, ACS Cent. Sci., 3 (2017), pp. 1137-1139. https://doi.org/10.1021/acscentsci.7b00469.
9. M.E. O'Reilly, R.S. Kim, S. Oh, Y. Surendranath, Catalytic Methane Monofunctionalization by an Electrogenerated High-Valent Pd Intermediate, ACS Cent. Sci. 3 (2017) 1174–1179. https://doi.org/10.1021/acscentsci.7b00342.
10. Y. Zhou, F. Che, M. Liu, C. Zou, Z. Liang, P. De Luna, H. Yuan, J. Li, Z. Wang, H. Xie, H. Li, P. Chen, E. Bladt, R. Quintero-Bermudez, T.-K. Sham, S. Bals, J. Hofkens, D. Sinton, G. Chen, E.H. Sargent, Dopant-induced electron localization

drives CO_2 reduction to C_2 hydrocarbons, Nat. Chem. 10 (2018) 974–980. https://doi.org/10.1038/s41557-018-0092-x.

11. P. De Luna, R. Quintero-Bermudez, C.-T. Dinh, M. B. Ross, O. S. Bushuyev, P. Todorović, T. Regier, S. O. Kelley, P. Yang, E. H. Sargent, Catalyst electro-redeposition controls morphology and oxidation state for selective carbon dioxide reduction, Nat. Catal. 1 (2018) 103–110. https://doi.org/10.1038/s41929-017-0018-9.
12. C.-T.Dinh, T.Burdyny, MD G. Kibria, A. Seifitokaldani, C.M. Gabardo, F. P.García De Arquer, A. Kianijonathan, J.P. Edwards, P. De Luna, O.S. Bushuyev, C. Zou, R. Quintero-Bermudez, Y. Pang, D. Sinton, E. H. Sargent, CO_2 electroreduction to ethylene via hydroxide-mediated copper catalysis at an abrupt interface, Science 360 (2018) 783–787. https://doi.org/10.1126/science.aas9100.
13. Loiudice, P. Lobaccaro,E. A. Kamali,T. Thao, B. H. Huang, J. W. Ager, R. Buonsanti, Tailoring copper nanocrystals towards C_2 products in electrochemical CO_2 reduction, Angew. Chem. Int. Ed. 55 (2016) 5789–5792. https://doi.org/10.1002/anie.201601582.
14. P. De Luna, C. Hahn, D. Higgins, S. A. Jaffer, T. F. Jaramillo, E. H. Sargent, 2019. What would it take for renewably powered electrosynthesis to displace petrochemical processes?, Science 364, eaav3506. https://doi.org/10.1126/science.aav3506.
15. O. S. Bushuyev, P. De Luna, C. T. Dinh, L. Tao, G. Saur, J. van de Lagemaat, S. O. Kelley, E. H. Sargent, What Should We Make with CO_2 and How Can We Make It?, Joule 2 (2018) 825–832. https://doi.org/10.1016/j.joule.2017.09.003.
16. J. M. Spurgeon, B. Kumar, A comparative technoeconomic analysis of pathways for commercial electrochemical CO_2 reduction to liquid products, Energy Environ. Sci. 11 (2018) 1536–1551. https://doi.org/10.1039/C8EE00097B.
17. J. Shan, M. Li, L.F. Allard, S. Lee, M. Flytzani-Stephanopoulos, Mild Oxidation of Methane to Methanol or Acetic Acid on Supported Isolated Rhodium Catalysts, Nature 551 (2017) 605−608. https://doi.org/10.1038/nature24640.
18. Y. Kwon, T.Y. Kim, G. Kwon, J. Yi, H. Lee, Selective Activation of Methane on Single-Atom Catalyst of Rhodium Dispersed on Zirconia for Direct Conversion, J. Am. Chem. Soc. 139 (2017) 17694−17699. https://doi.org/10.1021/jacs.7b11010.

19. Y. Chen, R. Guo, X. Peng, X. Wang, X. Liu, J. Ren, J. He, L. Zhuo, J. Sun, Y. Liu, Y. Wu, J. Luo, Highly Productive Electrosynthesis of Ammonia by Admolecule-Targeting Single Ag Sites, ACS Nano 14 (2020) 6938−6946. https://doi.org/10.1021/acsnano.0c01340.
20. L. Han, Z. Ren, P. Ou, H. Cheng, N. Rui, L. Lin, X. Liu, L. Zhuo, J. Song, J. Sun, J. Luo, H.L. Xin, Modulating single-atom palladium sites with copper for enhanced ambient ammonia electrosynthesis, Angew. Chem. Int. Ed. Engl. 60 (2021) 345-350. https://doi.org/10.1002/anie.202010159.
21. H. Liu, J. Fu, H. Li, J. Sun, X. Liu, Y. Qiu, X. Peng, Y. Liu, H. Bao, L. Zhuo, R. Cao, S. Zhang, J. Luo, Single palladium site in ordered porous heteroatom-doped carbon for high-performance alkaline hydrogen oxidation, Appl. Catal. B-Environ. 306 (2022) 121029. https://doi.org/10.1016/j.apcatb.2021.121029.
22. S. Liu, M. Jin, J. Sun, Y. Qin, S. Gao, Y. Chen, S. Zhang, J. Luo, X. Liu, Coordination environment engineering to boost electrocatalytic CO_2 reduction performance by introducing boron into single-Fe-atomic catalyst, Chem. Eng. J., 437 (2022) 135294. https://doi.org/10.1016/j.cej.2022.135294.
23. J. Xu, S. Lai, D. Qi, M.Hu, X. Peng, Y. Liu, W. Liu, G. Hu, H. Xu, F. Li, C. Li, J. He, L. Zhuo, J. Sun, Y. Qiu, S. Zhang, J. Luo, X. Liu, Atomic Fe-Zn dual-metal sites for high-efficiency pH-universal oxygen reduction catalysis, Nano Res. 14 (2021) 1374–1381. https://doi.org/10.1007/s12274-020-3186-x.
24. H. Bao, Y. Qiu, X. Peng, J.-a. Wang, Y. Mi, S. Zhao, X. Liu, Y. Liu, R. Cao, L. Zhuo, J. Ren, J. Sun, J. Luo, X. Sun, Isolated copper single sites for high-performance electroreduction of carbon monoxide to multicarbon products, Nat. Commun. 12 (2021). https://doi.org/10.1038/s41467-020-20336-4.
25. J.Wei, E. Iglesia. Structural requirements and reaction pathways in methane activation and chemical conversion catalyzed by rhodium, J. Catal. 225 (2004) 116–127. https://doi.org/10.1016/j.jcat.2003.09.030.
26. Y. Tang, Y. Li, V. Fung, D.-e. Jiang, W. Huang, S. Zhang, Y. Iwasawa, T. Sakata, L. Nguyen, X. Zhang, A. I. Frenkel, F. Tao, 2018. Single Rhodium Atoms Anchored in Micropores for Efficient Transformation of Methane under Mild Conditions. Nat. Commun. 9, 1231. https://doi.org/10.1038/s41467-018-03235-7.
27. Kokalj, N. Bonini, C. Sbraccia, S. de Gironcoli, S. Baroni, Engineering the Reactivity of Metal Catalysts: A Model Study of Methane Dehydrogenation on

Rh(111), J. Am. Chem. Soc. 126 (2004) 16732−16733. http://dx.doi.org/10.1021/ja045169h.

28. Y. Hori, I. Takahashi, O. Koga, N. Hoshi, Electrochemical reduction of carbon dioxide at various series of copper single crystal electrodes, J. Mol. Catal. A: Chem. 199 (2003) 39–47. https://doi.org/10.1016/S1381-1169(03)00016-5.
29. D. Ren, Y. Deng, A. D. Handoko, C. S. Chen, S. Malkhandi, B. S. Yeo, Selective electrochemical reduction of carbon dioxide to ethylene and ethanol on copper(I) oxide catalysts, ACS Catal. 5 (2015) 2814–2821. https://doi.org/10.1021/cs502128q.
30. Y. Lum, B. Yue, P. Lobaccaro, A. T. Bell, J. W. Ager, Optimizing C-C coupling on oxide-derived copper catalysts for electrochemical CO_2 reduction, J. Phys. Chem. C. 121 (2017) 14191–14203. https://doi.org/10.1021/acs.jpcc.7b03673.
31. F. S. Roberts, K. P. Kuhl, A. Nilsson, High selectivity for ethylene from carbon dioxide reduction over copper nanocube electrocatalysts, Angew. Chem. Int. Ed. 54 (2015) 5179–5182. https://doi.org/10.1002/ange.201412214.
32. Y. Song, R. Peng, D.K. Hensley, P. V. Bonnesen, L. Liang, Z. Wu, H. M. Meyer III, M. Chi, C. Ma, B. G. Sumpter, A. J. Rondinone, High-selectivity electrochemical conversion of CO2 to ethanol using a copper nanoparticle/N-doped graphene electrode, Chem. Sel. 1 (2016) 6055–6061. https://doi.org/10.1002/slct.201601169.
33. K. Jiang, R. B. Sandberg, A. J. Akey, X. Liu, D. C. Bell, J. K. Nørskov, K. Chan, H. Wang, Metal ion cycling of Cu foil for selective C-C coupling in electrochemical CO_2 reduction, Nat. Catal. 1 (2018) 111–119. https://doi.org/10.1038/s41929-017-0009-x.
34. H. Mistry, A. S. Varela, C. S. Bonifacio, I. Zegkinoglou, I. Sinev, Y.-W. Choi, K. Kisslinger, E. A. Stach, J. C. Yang, P. Strasser, B. R. Cuenya, 2016. Highly selective plasma-activated copper catalysts for carbon dioxide reduction to ethylene. Nat. Commun. 7, 12123. https://doi.org/10.1038/ncomms12123.
35. D. Gao, I. Zegkinoglou, N.J. Divins, F. Scholten, I. Sinev, P. Grosse, B. R. Cuenya, Plasma-activated copper nanocube catalysts for efficient carbon dioxide electroreduction to hydrocarbons and alcohols, ACS Nano 11 (2017) 4825–4831. https://doi.org/10.1021/acsnano.7b01257.
36. T.T. Zhuang, Z. Q. Liang, A. Seifitokaldani, Y. Li, P. De Luna, T. Burdyny, F. Che, F. Meng, Y. Min, R. Quintero-Bermudez, C. T. Dinh, Y. Pang, M. Zhong, B.

Zhang, J. Li, P.-N. Chen, X.L. Zheng, H. Liang, W.N. Ge, B. J. Ye, D. Sinton, S. H. Yu, E. H. Sargent, Steering post-C-C coupling selectivity enable high efficiency electroreduction of carbon dioxide to multi-carbon alcohols, Nat. Catal. 1 (2018) 421–428. https://doi.org/10.1038/s41929-018-0084-7.

37. Y. Song, W. Chen, C. Zhao, S. Li, W. Wei, Y. Sun, Metal-free nitrogen-doped mesoporous carbon for electroreduction of CO_2 to ethanol, Angew. Chem. Int. Ed. 56 (2017) 10840–10844. DOI:10.1002/anie.201706777.
38. E. L. Clark, C. Hahn, T. F. Jaramillo, A. T. Bell, Electrochemical CO_2 reduction over compressively strained CuAg surface alloys with enhanced multi-carbon oxygenate selectivity, J. Am. Chem. Soc. 139 (2017) 15848–15857. https://doi.org/10.1021/jacs.7b08607.
39. X. Dong, J. Lei, Y. Chen, H. Jiang, M. Zhang, Selective hydrogenation of acetic acid to ethanol on Cu-In catalyst supported by SBA-15, Appl. Catal. B, 244 (2019) 448-458. https://doi.org/10.1016/j.apcatb.2018.11.062
40. R. Passos, S. H. Pulcinelli, V. Briois, and C. V. Santilli, High surface area hierarchical porous Al_2O_3 prepared by the integration of sol–gel transition and phase separation, RSC Adv. 6 (2016) 57217–57226. https://doi.org/10.1039/C6RA11477F.
41. L. Samain, A. Jaworski, M. Edén, D. M. Ladd, D. K. Seo, F. J. Garcia-Garcia, U. Häussermann, Structural analysis of ´highly porous c-Al_2O_3, J. Solid State Chem. 217 (2014) 1–8. https://doi.org/10.1016/j.jssc.2014.05.004.
42. F. M. Segal, M. F. Correa, R. Bacani, B. Castanheira, M. J. Politi, S. Brochsztain, E. R. Triboni, 2018. A novel synthesis route of mesoporous c-alumina from polyoxohydroxide aluminum, Mater. Res. 21, e20170674. https://doi.org/10.1590/1980-5373-MR-2017-0674.
43. H. Robatjazi, D. Weinberg, D. F. Swearer, C. Jacobson, M. Zhang, S. Tian, L. Zhou, P. Nordlander, N. J. Halas, 2019. Metal-organic frameworks tailor the properties of aluminum nanocrystals, Sci. Adv. 5, eaav5340. DOI: 10.1126/sciadv.aav5340.
44. F. Wang, J. Ma, S. Xin, Q. Wang, J. Xu, C. Zhang, H. He, X. C. Zeng, 2020. Resolving the puzzle of single-atom silver dispersion on nanosized γ-Al_2O_3 surface for high catalytic performance, Nat. Commun. 11, 529. https://doi.org/10.1038/s41467-019-13937-1.

45. M. Sarno, M. Iuliano, S. De Pasquale, E. Ponticorvo, A new nano-catalyst for sawdust hydrolysis. Appl. Catal. A-Gen. 602 (2020) 117686. https://doi.org/10.1016/j.apcata.2020.117686.
46. J.C. Matsubu, V.N. Yang, P. Christopher, Isolated Metal Active Site Concentration and Stability Control Catalytic CO2 Reduction Selectivity, J. Am. Chem. Soc. 137 (2015) 3076–3084. https://doi.org/10.1021/ja5128133.
47. M. Dimitrijević, D. urošević, S. Milić, M. Sokić, R. Marković, Dissolution Of Copper From Smelting Slag By Leaching In Chloride Media, J. Min. Metall. Sect. B-Metall. 53 (3) B (2017) 407-412. https://doi.org/10.2298/JMMB170425016D.
48. N. Habbache, S. Djerad, L. Tifouti, Optimization of the operation conditions for NiO dissolution with different leachants, Process Eng. J. 1 (2017) 59–67.
49. Y. Yu, Q. Zhang, Q. Yao, Y. Zhan, M. Lu, L. Yang, C. Xu, J. Xie, J.Y. Lee, Learning from nature: introducing an epiphyte–host relationship in the synthesis of alloy nanoparticles by co-reduction methods, Chem. Commun. 50 (2014) 9765-9768. DOI: 10.1039/C4CC04132A.
50. M. Sarno, E. Ponticorvo, Continuous flow HER and MOR evaluation of a new Pt/Pd/Co nano electrocatalyst, Appl. Surf. Sci. 459 (2018) 105–113. 10.1016/j.apsusc.2018.07.209.
51. J.C. Matsubu, V.N. Yang, P. Christopher, Isolated metal active site concentration and stability control catalytic CO_2 reduction selectivity, J. Am. Chem. Soc. 137 (2015) 3076–3084. DOI: 10.1021/ja5128133.
52. J. Schumann, J. Kröhnert, E. Frei, R. Schlögl, A. Trunschke, IR-Spectroscopic Study on the Interface of Cu-Based Methanol Synthesis Catalysts: Evidence for the Formation of a ZnO Overlayer, Top. Catal. 60 (2017) 1735–1743. DOI 10.1007/s11244-017-0850-9.
53. D. Gamarra, A. Martínez- Arias, Preferential oxidation of CO in rich H_2 over CuO/CeO_2: *Operando*-DRIFTS analysis of deactivating effect of CO_2 and H_2O, J. Catal. 263 (2009) 189–195. https://doi.org/10.1016/j.jcat.2009.02.012.
54. K. Hadjiivanov, H. Knözinger, FTIR Study of Low-Temperature CO Adsorption on Cu-ZSM-5: Evidence of the Formation of $Cu^{2+}(CO)_2$ Species, J. Catal. 191 (2000) 480−485. doi:10.1006/jcat.1999.2805.
55. Z. Wang, W. Wu, X. Bian, Y. Wu, Synthesis and characterization of amorphous Al_2O_3 and γ-Al2O3 by spray pyrolysis, Green Process Synth. 5 (2016) 305–310. DOI 10.1515/gps-2015-0128.

56. Z. Zhang, Y. Zhu, H. Asakura, B. Zhang, J. Zhang, M. Zhou, Y. Han, T. Tanaka, A. Wang, T. Zhang, N. Yan, 2017. Thermally stable single-atom Pt/m-Al_2O_3 for selective hydrogenation and CO oxidation, Nat. Commun. 8, 16100. https://doi.org/10.1038/ncomms16100.
57. Y. Gao, X. Wu, R. Nord, H. Härelind, D. Weng, Sulphation and ammonia regeneration of Pt/MnOx-CeO2/Al_2O_3 catalyst for NOx-assisted soot oxidation, Catal. Sci. Technol. 8 (2018) 1621–1631. https://doi.org/10.1039/C8CY00027A.
58. M. Sarno, E. Ponticorvo, N. Funicello, S. De Pasquale, 2020. Methane electrochemical oxidation at low temperature on Rh single atom/NiO/V_2O_5 nanocomposite, Appl. Catal. A-Gen. 603, 117746. https://doi.org/10.1016/j.apcata.2020.117746.
59. H. Jeong, O. Kwon, B. S. Kim, J. Bae, S. Shin, H. E. Kim, J. Kim, H. Lee, Highly durable metal ensemble catalysts with full dispersion for automotive applications beyond single-atom catalysts, Nat. Catal. 3 (2020) 368–375. https://doi.org/10.1038/s41929-020-0427-z.
60. Liu, L. Liu, Y. Cao, J. Wang, R. Si, F. Gao, L. Dong, Controlling Dynamic Structural Transformation of Atomically Dispersed CuOx Species and Influence on Their Catalytic Performances, ACS Catal. 9 (2019) 9840−9851. https://doi.org/10.1021/acscatal.9b02773.
61. J. Zhang, C. Zheng, M. Zhang, Y. Qiu, Q. Xu, W. C. Cheong, W. Chen, L. Zheng, L. Gu, Z. Hu, D. Wang, Y. Li, Controlling N-doping type in carbon to boost single-atom site Cu catalyzed transfer hydrogenation of quinolone, Nano Res. 13 (2020) 3082–3087. https://doi.org/10.1007/s12274-020-2977-4.
62. R. Feng, S. Liu, P. Bai, K. Qiao, Y. Wang, H. A. Al-Megren, M. J. Rood, Z. Yan, Preparation and Characterization of γ-Al_2O_3 with Rich Brønsted Acid Sites and Its Application in the Fluid Catalytic Cracking Process, J. Phys. Chem. C 118 (2014) 6226–6234. https://doi.org/10.1021/jp411405r.
63. D.Y. Li, Y. S. Lin, Y.C. Li, D. L. Shieh, J. L. Lin, Synthesis of mesoporous pseudoboehmite and alumina templated with 1-hexadecyl-2,3-dimethyl-imidazolium chloride, Micropor. Mesopor. Mat. 108 (2008) 276–282. https://doi.org/10.1016/j.micromeso.2007.04.009.
64. P. Burtin, J.P. Brunelle, M. Pijolat, M. Soustelle, Influence of surface area and additives on the thermal stability of transition alumina catalyst supports. I: Kinetic data, Appl. Catal. 34 (1987) 225-238. 10.1016/S0166-9834(00)82458-6.

65. C. Morterra, G. Magnacca, A case study: surface chemistry and surface structure of catalytic aluminas, as studied by vibrational spectroscopy of adsorbed species, Catal. Today 27 (1996) 497-532. https://doi.org/10.1016/0920-5861(95)00163-8.
66. R. Feng, P. Bai, S. Liu, P. Zhang, X. Liu, Z. Yan, Z. Zhang, X. Gao, The application of mesoporous alumina with rich Bronsted acidic sites in FCC catalysts, Appl. Petrochem. Res. 4 (2014) 367–372. https://doi.org/10.1007/s13203-014-0073-y.
67. H. Knözinger, P. Ratnasamy, Catalytic Aluminas: Surface Models and Characterization of Surface Sites, Catal. Rev. 17 (1978) 31−70. https://doi.org/10.1080/03602457808080878.
68. Q. Wang, M. Kan, Q. Han, G. Zheng, 2021. Electrochemical Methane Conversion, Small Struct. 2, 2100037. DOI: 10.1002/sstr.202100037.
69. A. Tomita, J. Nakajima, T. Hibino, Direct Oxidation of Methane to Methanol at Low Temperature and Pressure in an Electrochemical Fuel Cell, Angew. Chem. Int. Ed. 47 (2008) 1462–1464. https://doi.org/10.1002/anie.200703928.
70. N. Spinner, W.E. Mustain, Electrochemical Methane Activation and Conversion to Oxygenates at Room Temperature, J. Electrochem. Soc. 160 (2013) F1275–F1281. https://doi.org/10.1149/2.071311jes.
71. M. Ma, B.J. Jin, P. Li, M.S. Jung, J.I. Kim, Y. Cho, S. Kim, J.H. Moon, J.H. Park Ultrahigh Electrocatalytic Conversion of Methane at Room Temperature, Adv. Sci. 4 (2017) 1700379. https://doi.org/10.1002/advs.201700379.
72. B. Lee, T. Hibino, Efficient and selective formation of methanol from methane in a fuel cell-type reactor, J. Catal. 279 (2011) 233-240. https://doi.org/10.1016/j.jcat.2010.12.020.
73. B. Lee, Y. Sakamoto, D. Hirabayashi, K. Suzuki, T. Hibino, Direct oxidation of methane to methanol over proton conductor/metal mixed catalysts, J. Catal. 271 (2010) 195–200. https://doi.org/10.1016/j.jcat.2010.01.011.
74. C. Oh, J. Kim, Y. Hwang, M. Ma, J. Park, Electrocatalytic methane oxidation on Co3O4- incorporated ZrO2 nanotube powder, Appl. Catal. B Environ. 283 (2021) 119653. https://doi.org/10.1016/j.apcatb.2020.119653.
75. J. Lee, J. Yang, J.H. Moon, Solar Cell-Powered Electrochemical Methane-to-Methanol Conversion with CuO/CeO2 Catalysts, ACS Energy Lett. 6 (2021) 893–899. https://doi.org/10.1021/acsenergylett.0c02553.

76. M. Ma, C. Oh, J. Kim, J.H. Moon, J.H. Park, Electrochemical CH4 oxidation into acids and ketones on ZrO2:NiCo2O4 quasi-solid solution nanowire catalyst, Appl. Catal. B Environ. 259 (2019), 118095. https://doi.org/10.1016/j.apcatb.2019.118095.
77. Y. Song, Y. Zhao, G. Nan, W. Chen, Z. Guo, S. Li, Z. Tang, W. Wei, Y. Sun, Electrocatalytic oxidation of methane to ethanol via NiO/Ni interface, Appl. Catal. B Environ. 270 (2020), 118888. https://doi.org/10.1016/j.apcatb.2020.118888.
78. K. Narsimhan, V. K. Michaelis, G. Mathies, W. R. Gunther, R. G. Griffin and Y. Román-Leshkov, Methane to Acetic Acid over Cu-Exchanged Zeolites: Mechanistic Insights from a Site-Specific Carbonylation Reaction, J. Am. Chem. Soc. 137 (2015) 1825. https://doi.org/10.1021/ja5106927.
79. A. Bhan, E. Iglesia, A Link between Reactivity and Local Structure in Acid Catalysis on Zeolites, Acc. Chem. Res. 41 (2008) 559. https://doi.org/10.1021/ar700181t.
80. C. H. Botchway, R. Tia, E. Adei, A. J. O'Malley, N. Y. Dzade, C. Hernandez-Tamargo, N. H. de Leeuw, 2020. Influence of Topology and Brønsted Acid Site Presence on Methanol Diffusion in Zeolites Beta and MFI, Catalysts 10, 1342. DOI:10.3390/catal10111342.
81. J. F. Haw, W. Song, D. M. Marcus, J. B. Nicholas, The Mechanism of Methanol to Hydrocarbon Catalysis, Acc. Chem. Res. 36 (2003) 317−326. DOI: 10.1021/ar020006o.
82. G. Wang, G. Cai, 2021. Cooperative catalytic effects between Brønsted and Lewis acid sites and kinetics for production of methyl methacrylate on SO_4^{2-}/TiO_2-SiO_2, Chem. Eng. Sci. 229, 116165. https://doi.org/10.1016/j.ces.2020.116165.
83. R. A. Periana, O. Mironov, D. Taube, G. Bhalla, C.J. Jones, Catalytic, Oxidative Condensation of CH_4 to CH_3COOH in One Step via CH Activation, Science 301 (2003) 814−818. DOI: 10.1126/science.1086466.
84. M. Zerella, S. Mukhopadhyay, A.T. Bell, Direct oxidation of methane to acetic acid catalyzed by Pd^{2+} and Cu^{2+} in the presence of molecular oxygen, Chem. Commun. (2004) 1948−1949. https://doi.org/10.1039/B405549G.
85. M.C. Zhou, H.T. Zhang, H.F. Ma, W.Y. Ying, Insight on mechanism of Sn modification in alumina supported RhSn catalysts for acetic acid hydrogenation to fuel-grade ethanol Fuel 203 (2017), 774−780. https://doi.org/10.1016/j.fuel.2017.03.063.

86. T. H. Tan, J. Scott, Y. H. Ng, R. A. Taylor, K.F. Aguey-Zinsou, R. Amal, Understanding Plasmon and Band Gap Photoexcitation Effects on the Thermal-Catalytic Oxidation of Ethanol by TiO_2-Supported Gold, ACS Catal. 6 (2016) 1870–1879. https://doi.org/10.1021/acscatal.5b02785.
87. J.M. Léger, S. Rousseau, C. Coutanceau, F. Hahn, C. Lamy, How bimetallic electrocatalysts does work for reactions involved in fuel cells?: example of ethanol oxidation and comparison to methanol, Electrochim. Acta, 50 (2005) 5118-5125. https://doi.org/10.1016/j.electacta.2005.01.051
88. J. Raskó, A. Hancz, A. Erdőhelyi, Surface species and gas phase products in steam reforming of ethanol on TiO_2 and Rh/TiO_2, Appl. Catal., A 269 (2004) 13−25. https://doi.org/10.1016/j.apcata.2004.03.053.

Click here to access/download;Figure;Figure_after revisions.docx

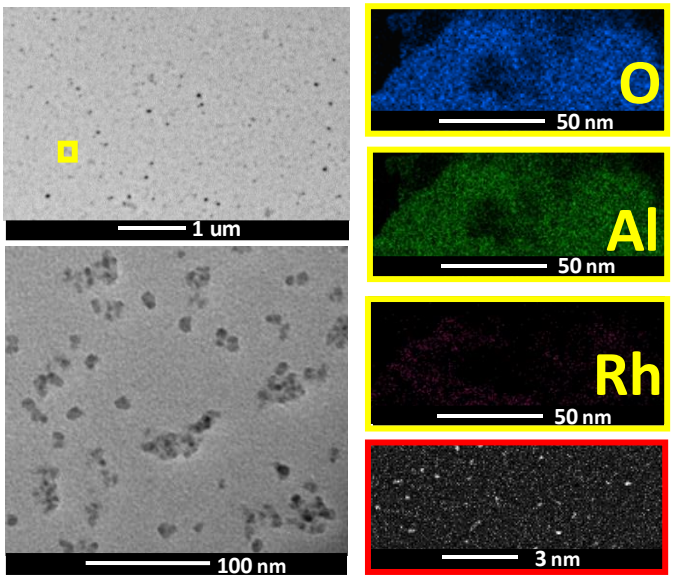

Figure 1. TEM images of Rh/Al_2O_3, aberration-corrected HAADF/STEM image (red box), and EDX maps of O, Al, and Rh (yellow boxes).

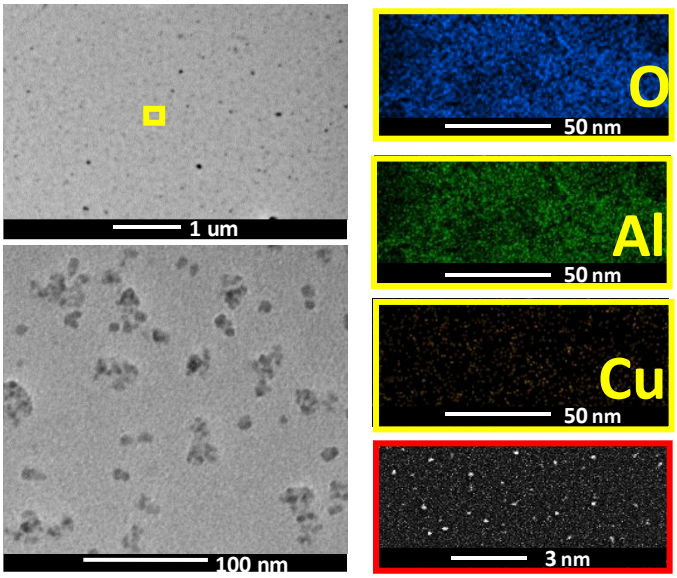

Figure 2. TEM images of Cu/Al_2O_3, aberration-corrected HAADF/STEM image (red box), and EDX maps of O, Al, and Cu (yellow boxes).

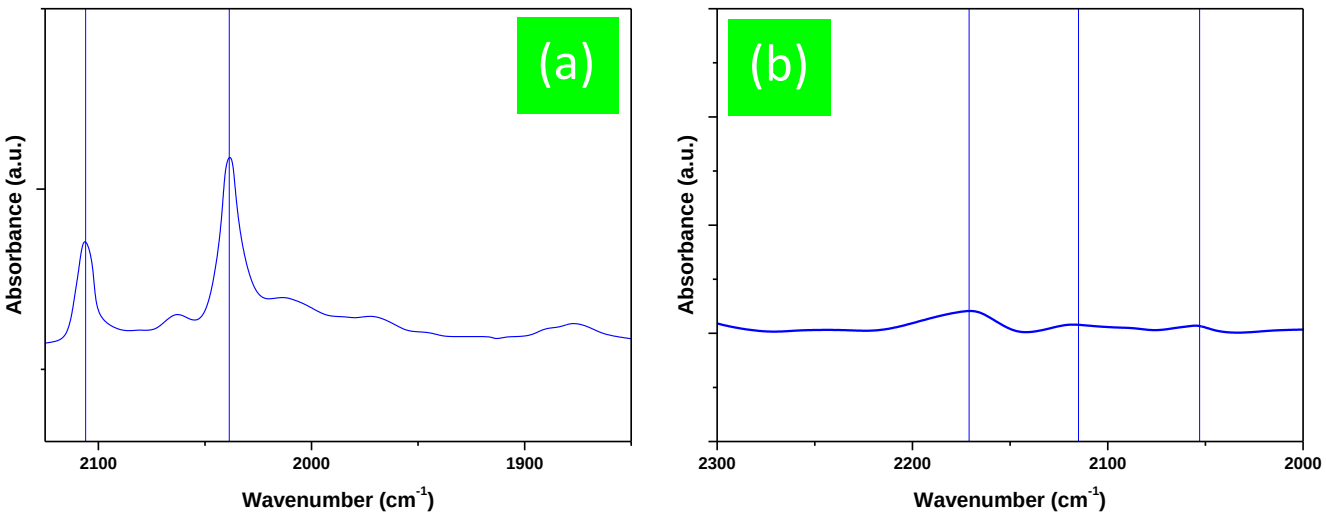

Figure 3. CO-DRIFTS spectra of Rh/Al_2O_3 (a) and Cu/Al_2O_3 (b).

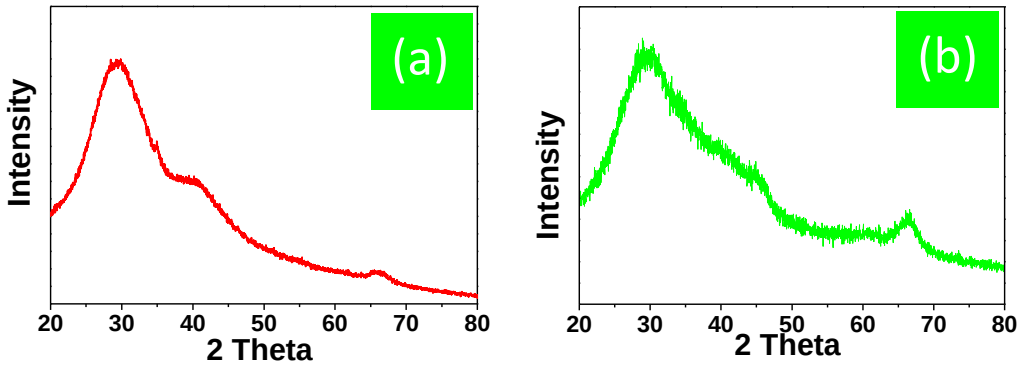

Figure 4. XRD spectra of Rh/Al_2O_3 (a) and Cu/Al_2O_3 (b).

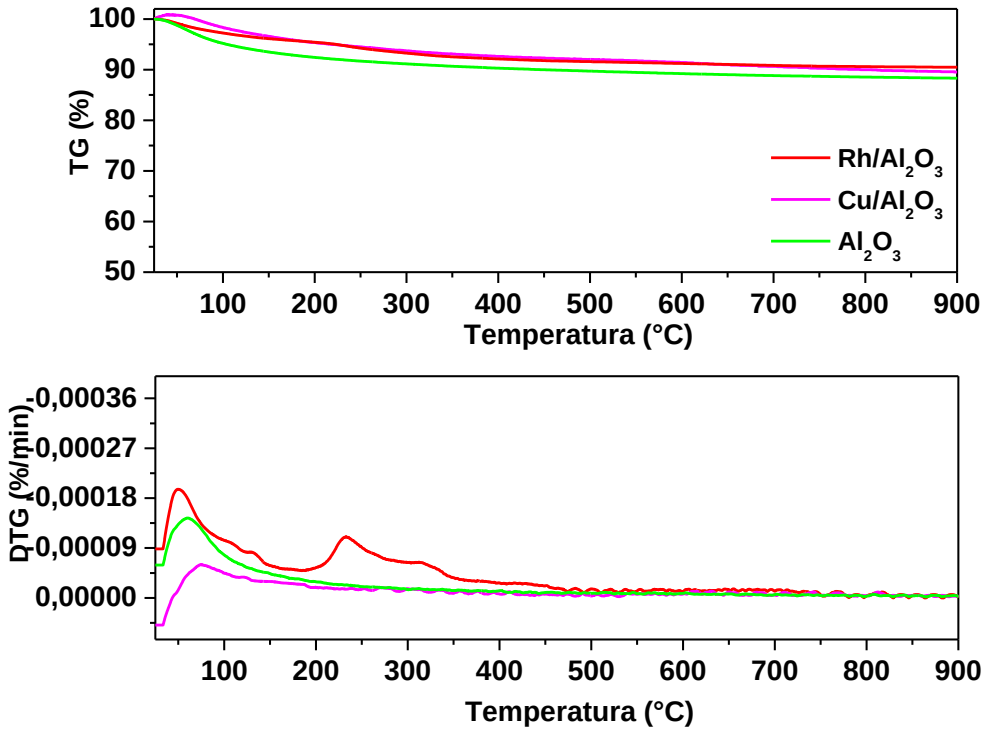

Figure 5. TG-DTG profiles of Al_2O_3 after calcination at 500°C, Rh/Al_2O_3, and Cu/Al_2O_3.

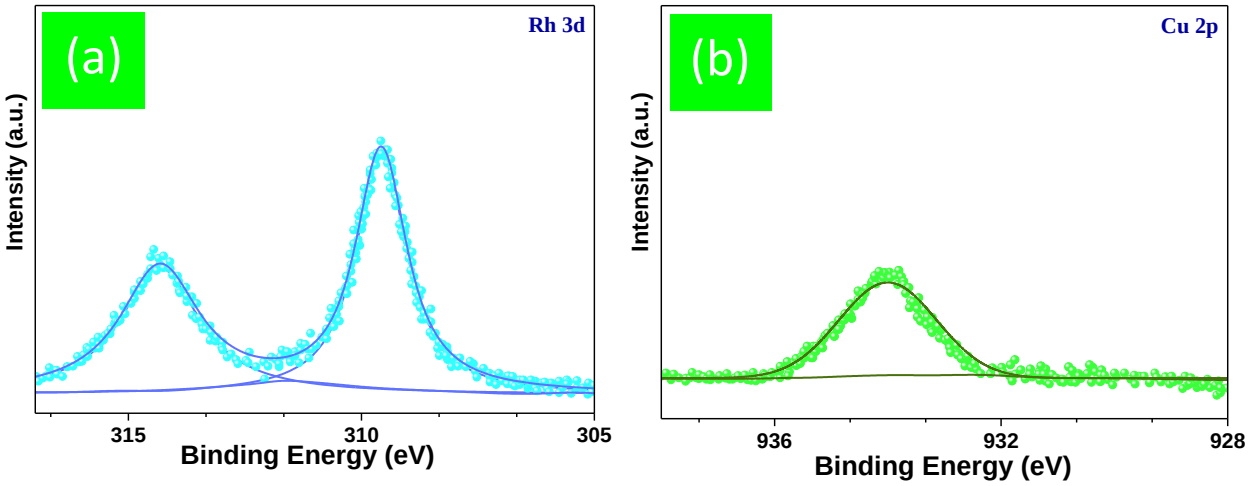

Figure 6. XPS spectra of Rh/Al_2O_3 and Cu/Al_2O_3: deconvoluted Rh 3d (a) and Cu 2p (b) spectra.

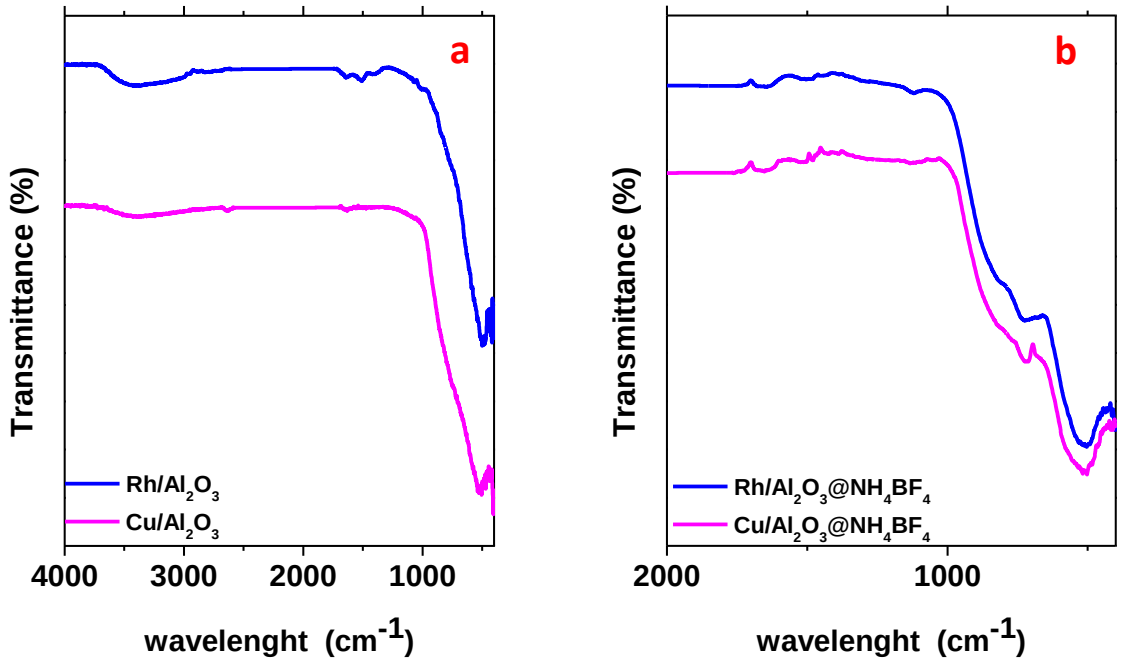

Figure 7. FT-IR spectra for Rh/Al_2O_3 and Cu/Al_2O_3 before the modification with NH_4BF_4 (a) and after NH_4BF_4 modification (b).

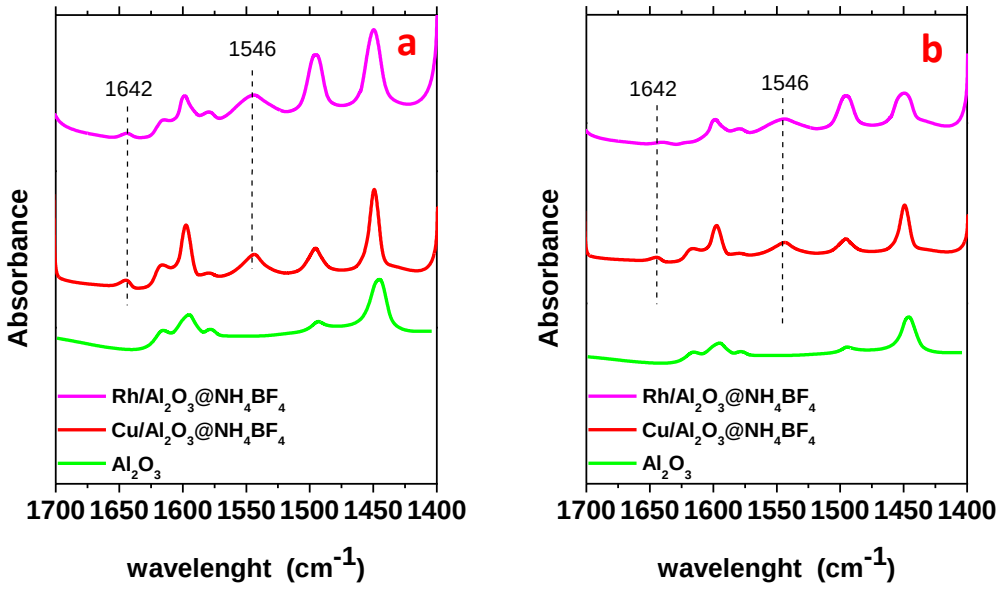

Figure 8. FT-IR spectra of adsorbed pyridine on Al_2O_3, Rh/Al_2O_3, and Cu/Al_2O_3 modified with NH_4BF_4. The samples are shown after exposure to pyridine and then treated under vacuum for 3 h (a), and after thermal heating at 300 °C for 1 h (b).

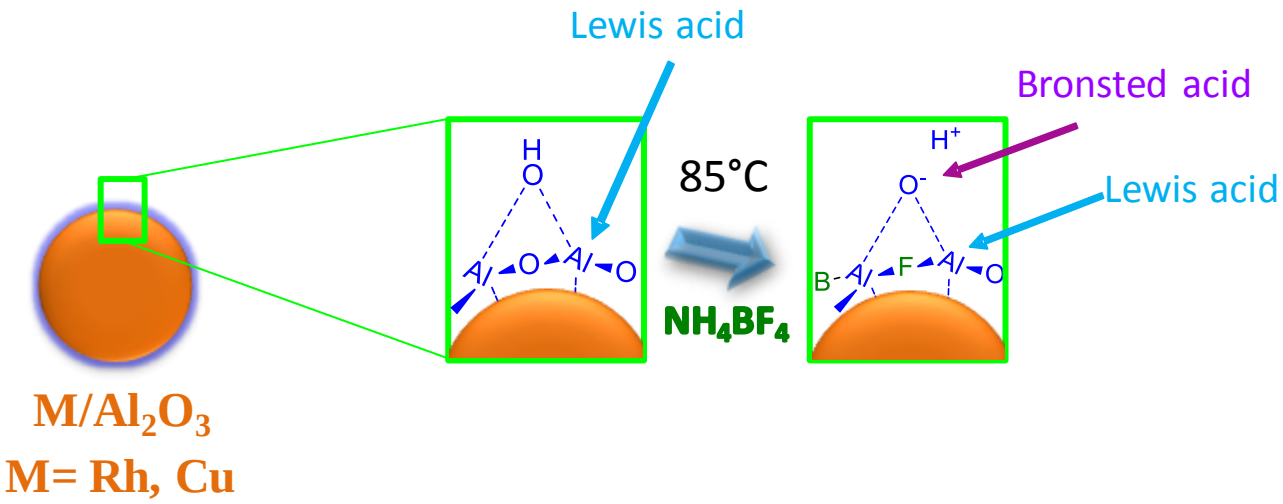

Figure 9. The schematic mechanism for the formation of Brønsted acid sites on the catalyst surface.

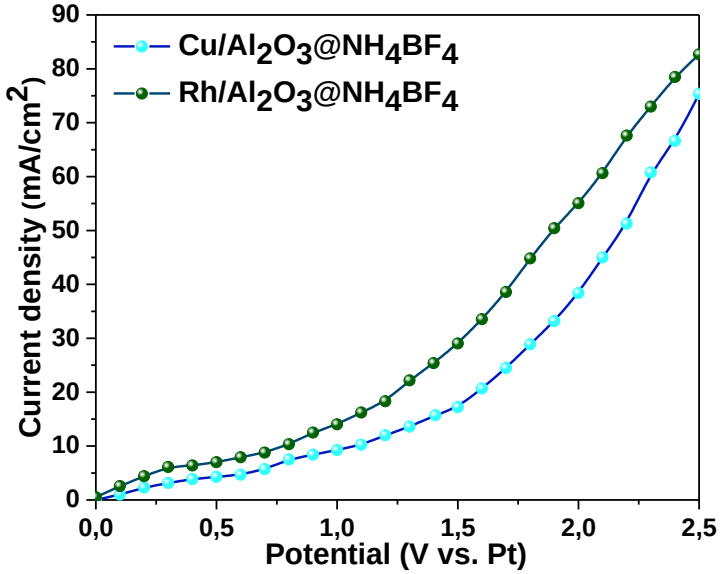

Figure 10. Electrochemical performance of CH_4 oxidation: LSV curves, at 20 mV/s, of Rh/Al_2O_3 and Cu/Al_2O_3 modified with NH_4BF_4.

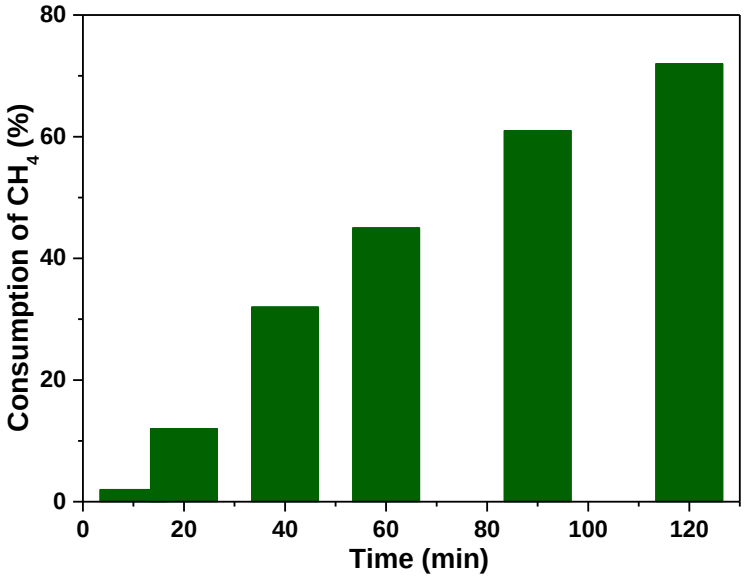

Figure 11. Consumption ratio of CH_4 after 10, 20, 40, 60, 90 and 120 minutes of CH_4 electrochemical conversion by Rh/Al_2O_3 modified with NH_4BF_4.

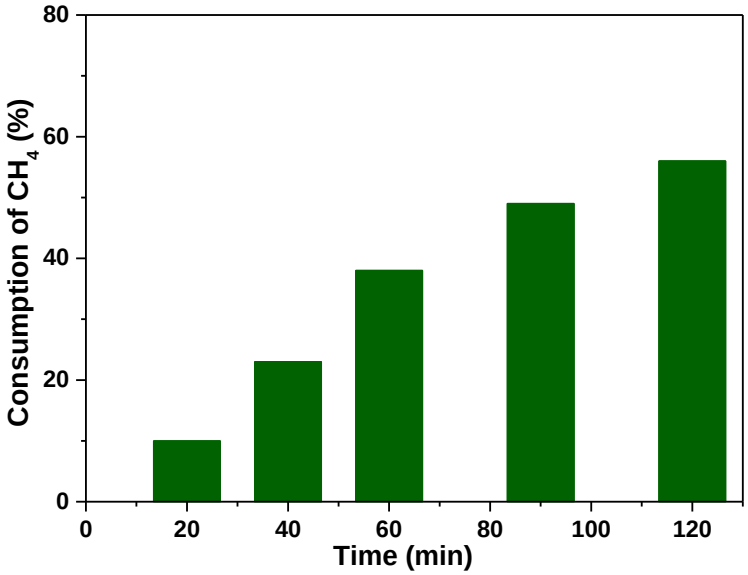

Figure 12. Consumption ratio of CH_4 after 20, 40, 60, 90 and 120 minutes of CH_4 electrochemical conversion by Cu/Al_2O_3 modified with NH_4BF_4.

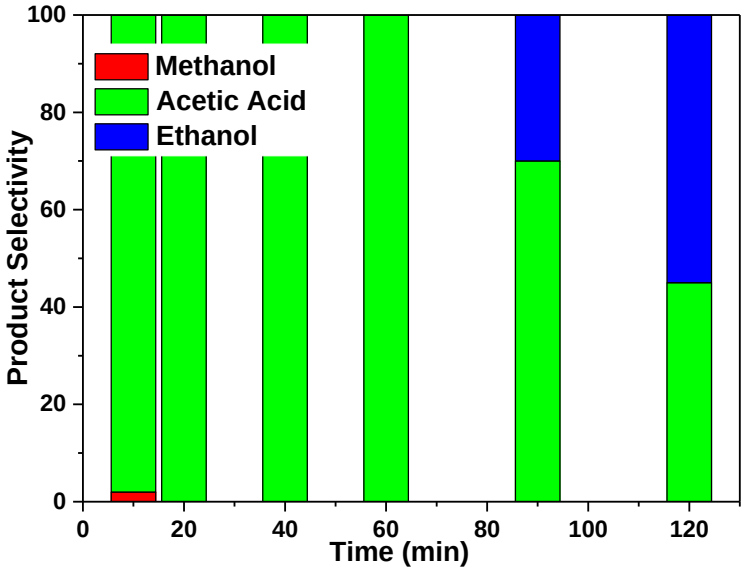

Figure 13. Product selectivity after 10, 20, 40, 60, 90, and 120 minutes of CH_4 electrochemical conversion by Rh/Al_2O_3 modified with NH_4BF_4.

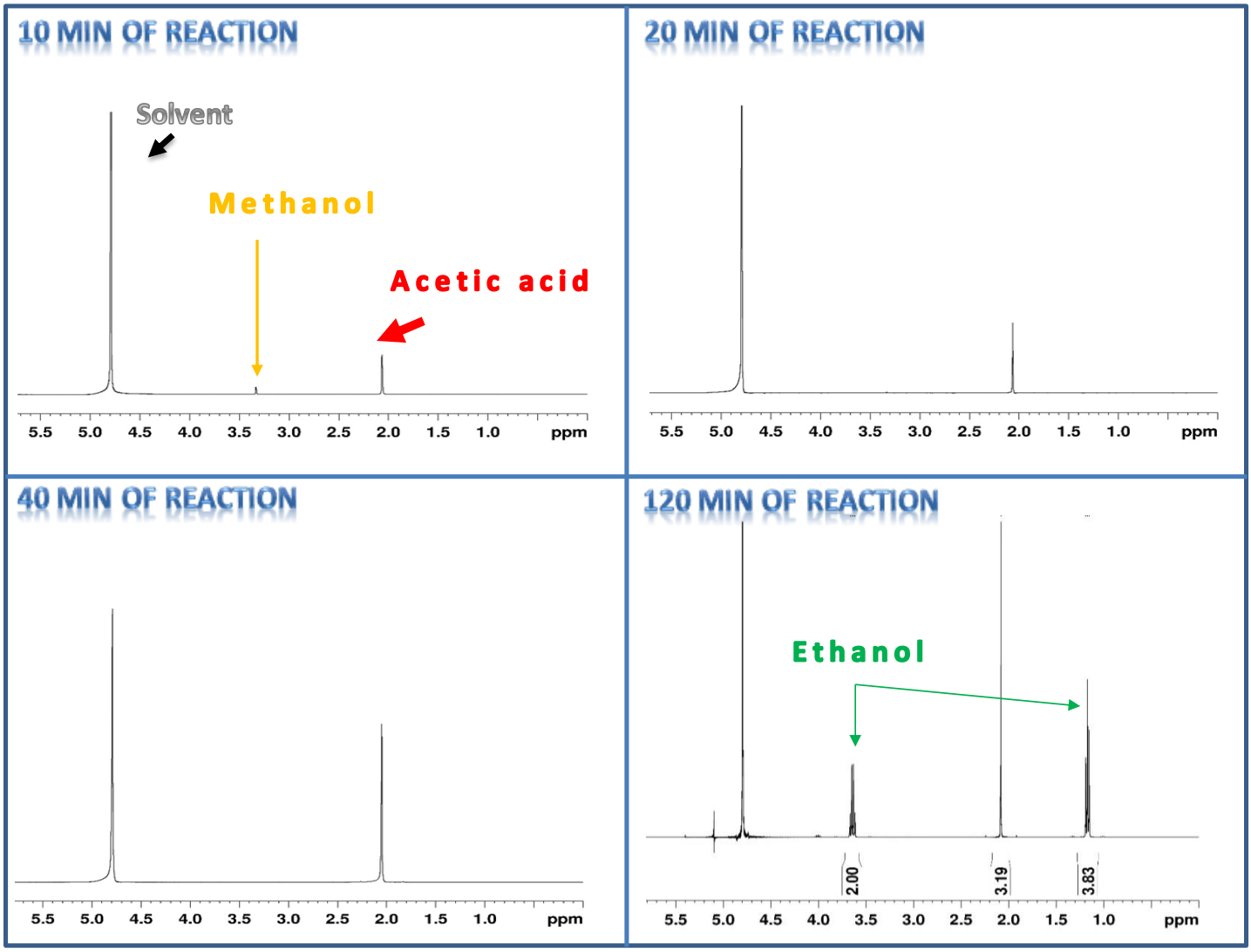

Figure 14. ^{1}H-NMR spectra of the products after 10, 20, 40, and 120 min of electrochemical CH_4 oxidation by Rh/Al_2O_3 modified with NH_4BF_4.

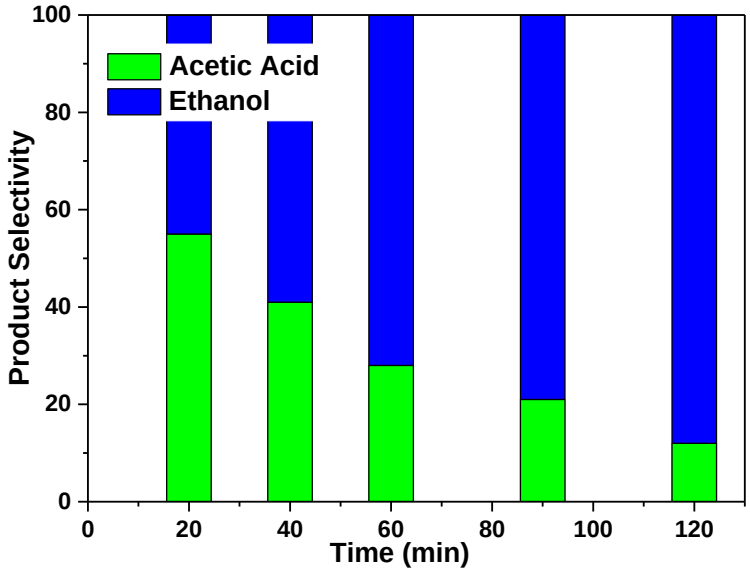

Figure 15. Product selectivity after 20, 40, 60, 90, and 120 minutes of CH_4 electrochemical conversion by Cu/Al_2O_3 modified with NH_4BF_4.

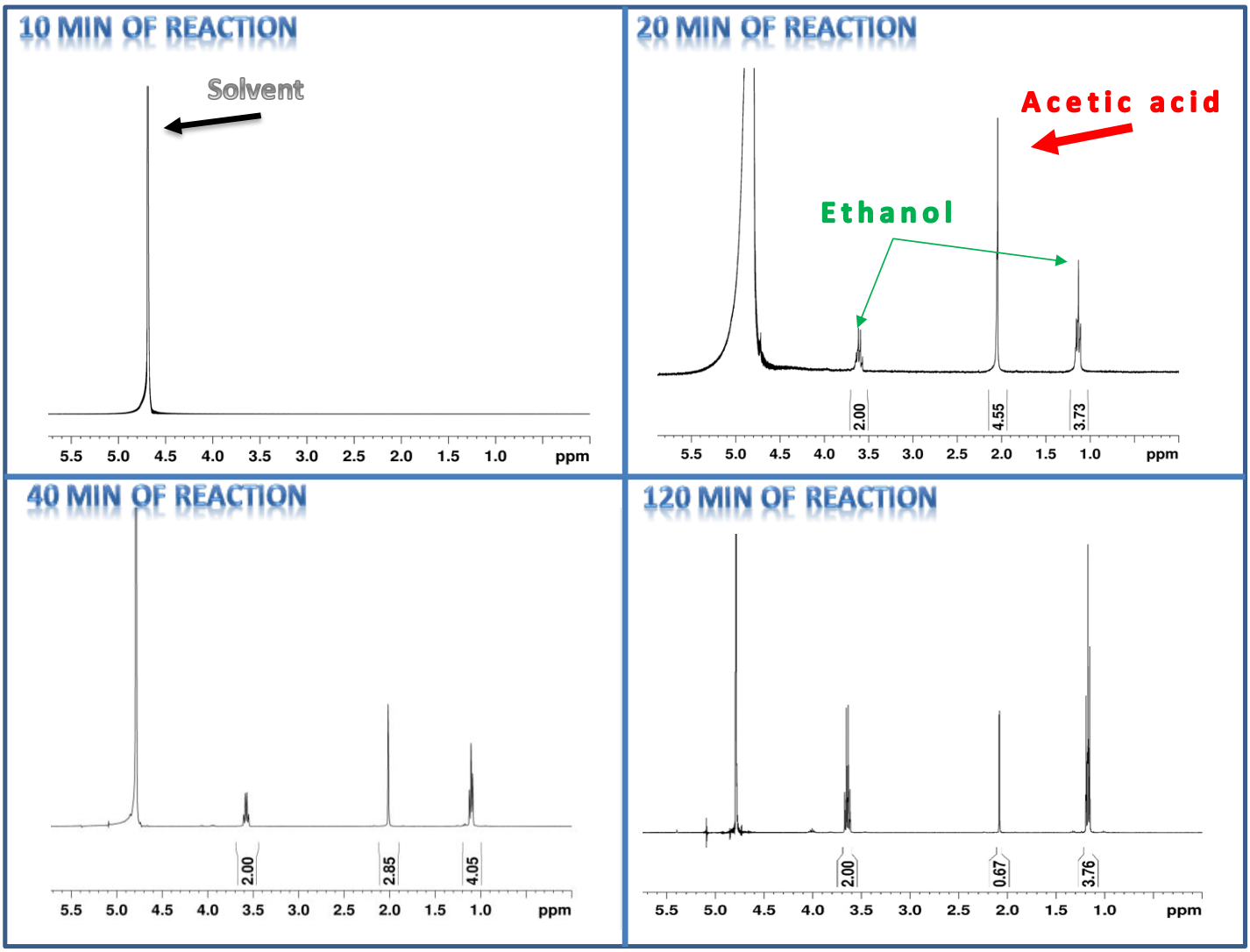

Figure 16. ^{1}H-NMR spectra of the products after 10, 20, 40, and 120 min of electrochemical CH_4 oxidation conversion by Cu/Al_2O_3 modified with NH_4BF_4.

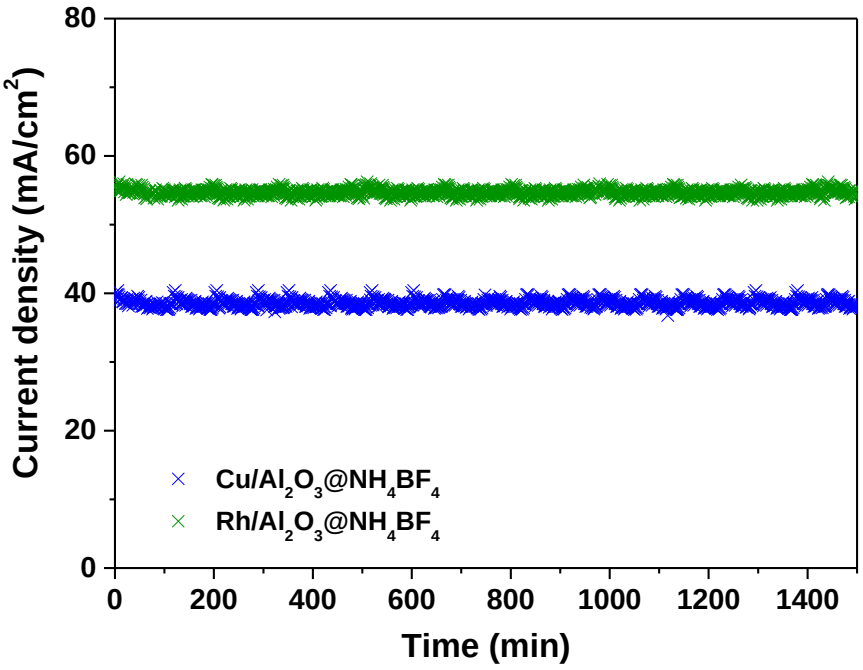

Figure 17. Current density-time curves of Rh/Al_2O_3 and Cu/Al_2O_3 modified with NH_4BF_4, during long term electrochemical CH_4 oxidation.

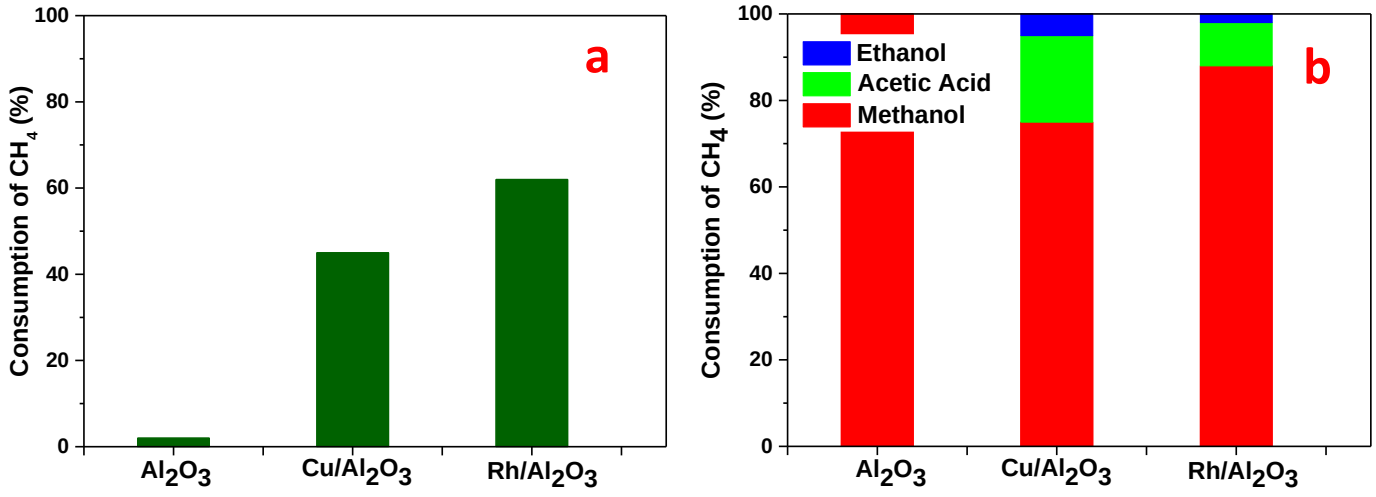

Figure 18. Consumption ratio of CH_4 by Rh/Al_2O_3, Cu/Al_2O_3, and Al_2O_3 before the modification with NH_4BF_4 (a), product selectivity by Rh/Al_2O_3, Cu/Al_2O_3, and Al_2O_3 before the modification with NH_4BF_4 (b); after 120 minutes of CH_4 electrochemical conversion.

Table 1. Comparison of the performances between Rh/Al_2O_3 and Cu/Al_2O_3 modified with NH_4BF_4 and the most performing electro-catalysts reported in the literature.

Electrocatalyst	T [°C]	Electrolytes	Electrolysis Condition	Main products	Yield	Current Efficiency	Ref.
Pd-Au/C	50	$Sn_{0.9}In_{0.1}P_2O_7$	400 mA/cm2	**CH_3OH**	~0.13 µmol/ h cm^2	_	**[69]**
$NiO-ZrO_2$	25	0.1 M Na_2CO_3	2.0 V	**CH_3OH, HCHO, CO**	_	_	**[70]**
ZrO_2/Co_3O_4	25	0.5 M Na_2CO_3	2.0 V	**$CH_3CH_2CH_2OH$, $CH_3CH(OH)CH_3$, CH_3CHO**	Not specified	_	**[71]**
V_2O_5/SnO_2	100	$Sn_{0.9}In_{0.1}P_2O_7$	0.8 V	**CH_3OH**	_	61.4	**[72]**
$NiO-V_2O_5/Rh$	100	Nafion membrane	25 mA/cm2	**CH_3OH**	5.2 µmol/ h cm^2	91	**[58]**
Pt–Au–Cu/C	300	$Sn_{0.9}In_{0.1}P_2O_7$	0.02 V	**CH_3OH**	Not specified	_	**[73]**
Co_3O_4/ZrO_2	40	0.5 M Na_2CO_3	1.6 V	**$CH_3CH_2CH_2OH$, $CH_3CH(OH)CH_3$**	2416 $\mu mol_{CH3CH2CH2OH}$ /g h	_	**[74]**
CuO/CeO_2	25	0.5 M Na_2CO_3	1.5 V	**CH_3OH**	753 µmol/g h	_	**[75]**
$NiCo_2O_4/ZrO_2$	25	0.5 M Na_2CO_3	**2.0 V**	**$CH_3CH_2CH_2OH$, $CH_3CH(OH)CH_3$ CH_3CH_2COOH**	1173 $\mu mol_{CH_3CH_2COOH}$ /g h	_	**[76]**
NiO/Ni	25	0.1 M NaOH	**1.4 V**	**CH_3CH_2OH**	25 µmol /g h	89	**[77]**
$Cu/Al_2O_3@NH_4BF_4$	25	0.5 M $KHCO_3$	**2.0 V**	**CH_3CH_2OH, CH_3COOH**	37.14 $\mu mol_{CH3CH2OH}$ /h cm^2	90	**This work**
$Rh/Al_2O_3@NH_4BF_4$	25	0.5 M $KHCO_3$	**2.0 V**	**CH_3CH_2OH, CH_3COOH**	33.57 $\mu mol_{CH3COOH}$ /h cm^2	95	**This work**

Supporting Info

SELECTIVE C2 ELECTROCHEMICAL SYNTHESIS FROM METHANE ON MODIFIED ALUMINA SUPPORTING SINGLE ATOM CATALYSTS

Eleonora Ponticorvo[1,2*], Mariagrazia Iuliano[3], Claudia Cirillo[1,2], Maria Sarno[1,2]

[1]Department of Physics "E.R. Caianiello" University of Salerno, Via Giovanni Paolo II ,132 - 84084 Fisciano (SA), Italy.

[2]NanoMates, Research Centre for Nanomaterials and Nanotechnology at the University of Salerno, University of Salerno, Via Giovanni Paolo II ,132 - 84084 Fisciano (SA), Italy.

[3]Department of Industrial Engineering, University of Salerno, via Giovanni Paolo II, 132 - 84084 Fisciano (SA), Italy

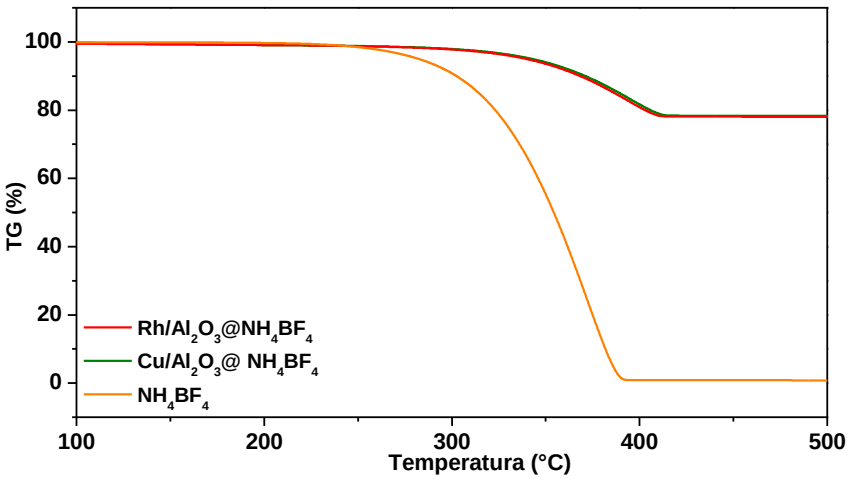

Figure S1. TG profiles of NH_4BF_4 alone, Rh/Al_2O_3, and Cu/Al_2O_3 after modification with NH_4BF_4.

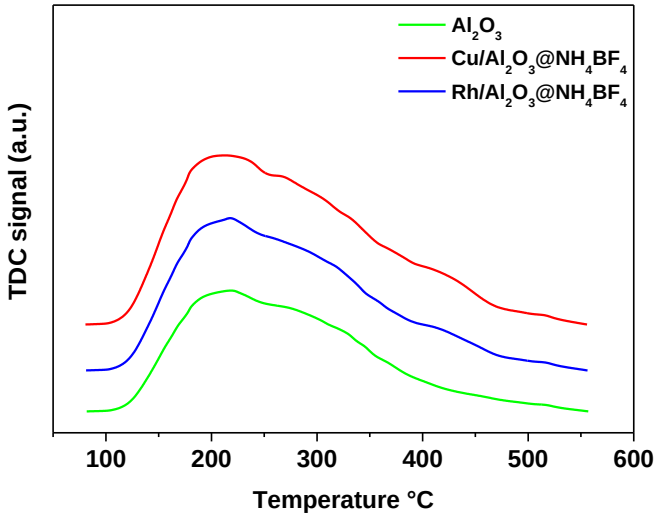

Figure S2. Temperature-programmed desorption of ammonia (NH_3-TPD) profiles.

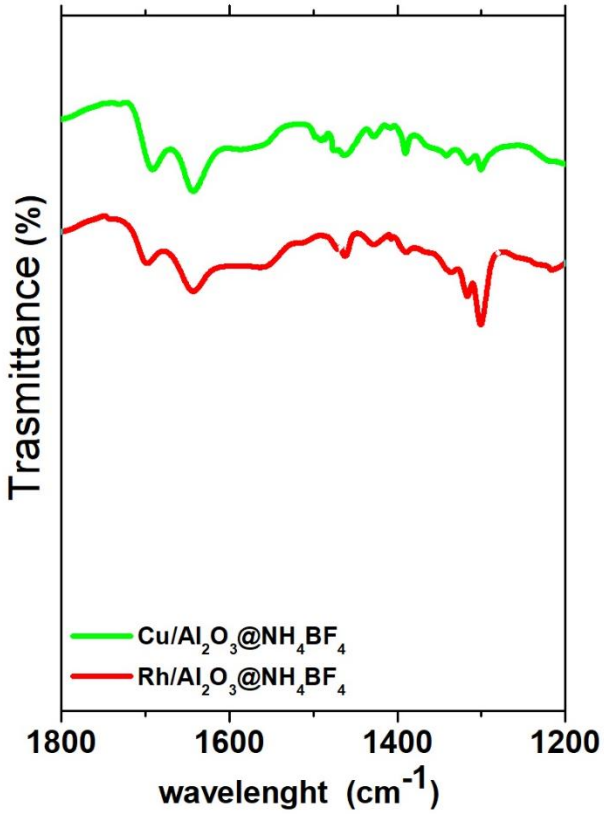

Figure S3. FTIR spectra of Cu/Al_2O_3 and Rh/Al_2O_3 modified with NH_4BF_4 after 90 min of CH_4 electrochemical conversion.

Graphical Abstract

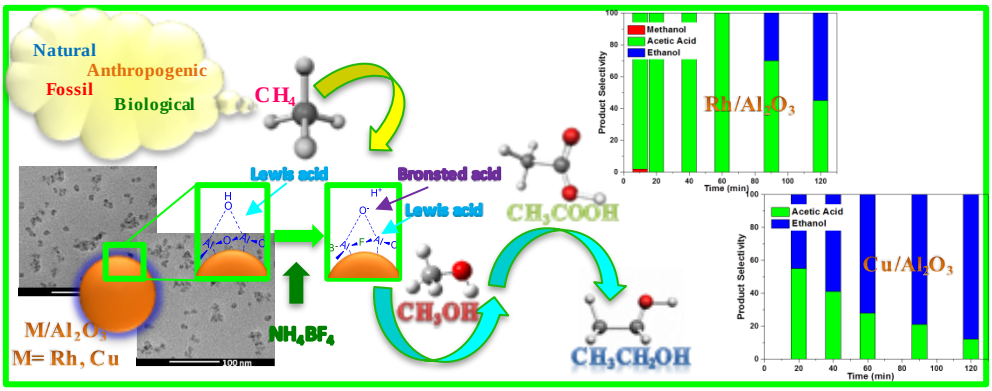

Highlights

- *A large amount of methane on the earth*
- *Aluminum oxide support*
- *Activity and selectivity of Rh and Cu single atoms supported catalyst*
- *Direct electrochemical oxidation of methane*
- *High and selective acetic acid and ethanol production*